PHYSICAL REVIEW A VOLUME 40, NUMBER 5 SEPTEMBER 1, 1989

Mass transport and mixing by modulated traveling waves

Jeffrey B. Weiss* and Edgar Knobloch
Physics Department, University of California, Berkeley, California 94720
(Received 28 September 1988)

Particle transport and mixing in modulated traveling waves in a binary-fluid mixture heated from below is studied numerically. The fluid divides into three regions separated by Kolmogorov-Arnol'd-Moser curves: a core region where particles are carried along with the wave (trapped), an outer region where particles are left behind by the wave (untrapped), and a separatrix layer between the two where particles chaotically alternate between being trapped and untrapped. The probability distributions for the lengths of individual trapped and untrapped events are sharply peaked at small times, have a power-law decay, and exhibit similar complex structure. The core and outer regions are responsible for long-range transport with no diffusion. The chaotic separatrix layer gives rise to long-range transport with enhanced mixing and anomalous diffusion, where, for long times $\langle x^2(t)\rangle - \langle x(t)\rangle^2 \sim t^\nu$, $1<\nu<2$.

I. INTRODUCTION

Hydrodynamic waves are of fundamental importance in many branches of physics, and both linear and nonlinear waves have been extensively studied. Less well studied, however, are the mixing and transport properties of such waves, which require a Lagrangian description. As is well known, linear waves do not cause mass transport; nonlinearities are required to produce a nonvanishing Stokes drift.[1,2] In addition, wave momentum or energy are transported if the waves break or dissipate. In the present paper we point out that quite simple waves may cause the fluid elements through which they pass to execute complex or chaotic motions leading to enhanced mixing and long-range transport. Such mixing occurs only in the coarse-grained sense, however, since fine mixing requires diffusion processes at the molecular level. These processes, which allow interchange of mass between neighboring fluid elements, are absent at the level of idealization represented by the equations of hydrodynamics. At this level the problem, may, therefore, be formulated in terms of fluid elements, hereafter referred to as "particles," which retain their identity during motion.

To make the above suggestion more concrete we focus on two-dimensional quasiperiodic waves in an incompressible fluid. Then the equations of motion for the particle trajectories can be written in the form of Hamilton's equations,[3]

$$\dot{x} = -\frac{\partial \psi(x,z,t)}{\partial z}, \quad \dot{z} = \frac{\partial \psi(x,z,t)}{\partial x}, \tag{1}$$

where x,z are, respectively, the horizontal and vertical coordinates and ψ is the stream function of the flow. In Eq. (1) the physical space occupied by the fluid is the phase space of the system, and the stream function is the Hamiltonian. If the stream function is time dependent then the particle trajectories may be chaotic even though the Eulerian flow is laminar.[3] Such a flow is said to display Lagrangian turbulence or chaotic advection. The simplest such example arises when ψ is periodic in time. Moreover, when ψ can be written in the form $\psi(x,z,t)=\psi_0(x,z)+\delta\psi_1(x,z,t)$, $\delta \ll 1$, the resulting particle motion is close to being integrable and homoclinic or heteroclinic orbits present in the integrable case may be broken. In this case it is possible to use ideas from Hamiltonian dynamics to investigate the structure of regular and chaotic regions in the fluid, and to show how this structure is responsible for the transport and mixing properties. When Eq. (1) describes motion in a quasiperiodic wave, the above discussion applies to a suitably defined *comoving* stream function. Consequently, the phenomena described in this paper are quite general, and are expected to be of relevance to two-dimensional quasiperiodic waves in a variety of physical systems.

We focus on waves in binary fluid convection: a two-species fluid mixture heated from below. This choice of system is suggested by recent experiments[4-6] which reveal not only convection in the form of traveling waves (TW), but also a secondary bifurcation from TW to modulated waves[5] (MW). Although the latter bifurcation occurs in spatially confined waves, its characteristics agree remarkably well with theoretical predictions[7] based on the assumption that the wave trains are spatially periodic. These predictions make use of equivariant bifurcation theory to analyze the system near a particular codimension-two bifurcation, and enable one to determine explicitly the TW and MW stream functions and thereby the conditions for the existence of chaotic particle trajectories in the MW.[8] In the present paper we use these results to study the role of chaotic advection in transport and mixing by modulated traveling waves. This study is complemented by more recent experiments investigating particle transport in TW,[6] and in time-dependent Rayleigh-Bénard convection.[9]

Earlier studies of transport in Hamiltonian systems have emphasized transport in the action variable. In contrast, the transport which arises in waves exhibiting

chaotic advection takes place in physical space, and occurs despite restriction of the motion to a very small range of action. This transport is similar to that studied by Geisel *et al.*, in a model of a two-dimensional solid.[10]

In Sec. II we describe the TW and MW stream functions and in Sec. III we give an overview of the transport and mixing properties of the waves. The chaos gives rise to episodic trapping and untrapping of particles, in which particles chaotically alternate between being carried with the wave and being left behind, resulting in long-range transport and enhanced mixing. In Sec. IV we investigate the stable and unstable manifolds of fixed points of an appropriately defined time-T map and discuss their role in the transport process. In Sec. V we use a surface of section map, the separatrix map, to study the trapping and untrapping processes in more detail. The use of these techniques is validated by detailed comparison with solutions to Eq. (1). In Sec. VI we investigate the phenomenon of anomalous diffusion which results from the existence of cantori, invariant curves which act as partial barriers to the particle trajectories. Our results are discussed in Sec. VII.

II. TRAVELING AND MODULATED WAVES

The waves which we study take the form of traveling rolls, i.e., they have a two-dimensional structure in the horizontal and vertical directions, with translation invariance in the remaining horizontal direction. We shall use the coordinates ξ, the horizontal position in a frame comoving with the TW, scaled such that the TW has wavelength 2π, and ζ the vertical position, scaled such that the bottom and top of the fluid are at $\zeta=0,\pi$, respectively. The time τ is chosen such that the TW has unit phase velocity.

In this comoving frame, the TW stream function is independent of time,[8]

$$\psi_0(\xi,\zeta)=-\zeta+R\cos\xi\sin\zeta\ , \tag{2}$$

and depends on a single parameter, the TW amplitude R. Equation (2) describes a traveling wave which, in the laboratory frame, moves to the left with unit phase speed. In the equations of motion for the particle trajectories, ψ_0 plays the role of a two-dimensional autonomous Hamiltonian. Such a Hamiltonian is integrable;[11,12] hence the particles travel along streamlines or surfaces of constant energy. The TW stream function for $R=3.266$ is shown in Fig. 1. At this value of R a secondary bifurcation to MW takes place.[8] Since the TW is periodic in ξ we may take the phase space to be the cylinder $\{(\xi,\zeta):\xi\in(-\pi,\pi),\zeta\in(0,\pi)\}$. The number of times a trajectory winds around the cylindrical phase space does, however, have direct physical significance. Two points which differ in ξ by $2\pi n$, where is n an integer, obey the same dynamics, but are in different parts of the wave train. We shall distinguish these different positions by their wave-crest number: $\xi\in(-\pi,\pi)$ has wave crest 0, $\xi\in(\pi,3\pi)$ has wave crest 1, etc. Observe that for $R>1$, ψ_0 contains two types of orbits: those which appear as closed curves, and those which wind around the cylinder, incrementing their wave-crest number. The regions containing these two types of trajectories are separated by heteroclinic orbits connecting pairs of saddle points which appear on $\zeta=0,\pi$ as R increases through unity. These special orbits are of particular interest in what follows.

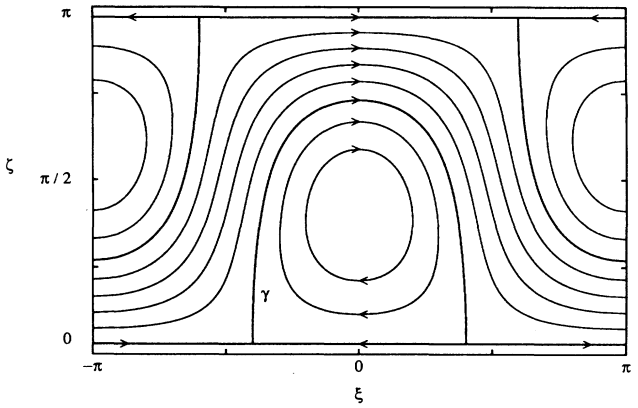

FIG. 1. The comoving stream lines in a pure traveling wave for $R=3.266$, showing the heteroclinic orbit γ separating regions of trapped and untrapped particles.

Near the secondary bifurcation the MW stream function ψ contains a small amplitude time-dependent perturbation[8]

$$\psi(\xi,\zeta,\tau)=\psi_0(\xi,\zeta)+\delta\psi_1(\xi,\zeta,\tau),\quad \delta\ll 1\ , \tag{3}$$

where

$$\psi_1(\xi,\zeta,\tau)=\frac{1}{2}\left[\left[1-\frac{2}{\alpha}\right]\cos(\xi+\alpha\tau+\theta)+\left[1+\frac{2}{\alpha}\right]\cos(\xi-\alpha\tau-\theta)\right]\sin\zeta\ . \tag{4}$$

The perturbation contains three parameters: the amplitude δ, the ratio α of the modulation frequency to the TW frequency, and a phase θ. The period of ψ_1 is $T=2\pi/\alpha$. We shall use the value of α deduced from the experiment,[5] $\alpha=0.195$, and without loss of generality take $\theta=0$.

The particle trajectories in the flow described by the MW stream function (3) are precisely those of an integrable Hamiltonian with a small amplitude nonintegrable Hamiltonian perturbation, and are given by

$$\begin{aligned}\xi_\tau&=1-R\cos\xi\cos\zeta-\frac{\delta}{2}\left[\left[1-\frac{2}{\alpha}\right]\cos(\xi+\alpha\tau)+\left[1+\frac{2}{\alpha}\right]\cos(\xi-\alpha\tau)\right]\cos\zeta\ ,\\ \zeta_\tau&=-R\sin\xi\sin\zeta-\frac{\delta}{2}\left[\left[1-\frac{2}{\alpha}\right]\sin(\xi+\alpha\tau)+\left[1+\frac{2}{\alpha}\right]\sin(\xi-\alpha\tau)\right]\sin\zeta\ .\end{aligned} \tag{5}$$

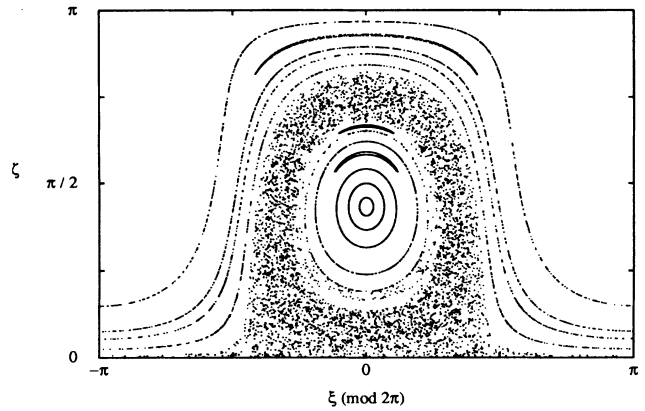

FIG. 2. Time-T map for a modulated wave with $R=3.266$, $\alpha=0.195$, $\theta=0$, and $\delta=0.4$. Several initial conditions were started along the line $\xi=0$.

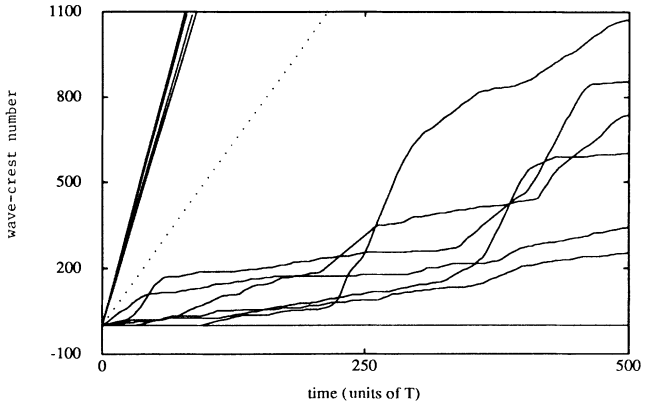

FIG. 3. Wave-crest number vs time for MW trajectories: the solid lines are particle trajectories, and the dotted line is a point fixed in the laboratory frame. The parameters are those used in Fig. 2.

As δ is increased from zero, we expect the appearance of hierarchies of island chains, successive breakup of Kolmogorov-Arnol'd-Moser (KAM) curves, and the appearance and thickening of chaotic layers.[11,12] Figure 2 is the time-T map when $\delta=0.4$, obtained by numerically integrating the MW equations of motion (5) for several initial conditions along the line $\xi=0$. The flow in the empty upper corners can be obtained from that in the lower center by the symmetry $\xi\to\xi+\pi$, $\zeta\to\pi-\zeta$. The large chaotic layer results from the breaking of the TW heteroclinic orbit. Three thin islands are visible, one of which is embedded in the chaotic layer. There are both chaotic layers and additional island chains within the regular regions, but they were not found by the initial conditions used in Fig. 2. These structures are typical of nonintegrable Hamiltonian systems.

The fluid in the MW is divided into three regions. In the core region particles are trapped and carried along with the wave. In the outer region particles are untrapped and left behind by the wave. These two regions are also present in the TW.[8] Between the core and the outer region is a chaotic separatrix layer bounded by KAM curves. The dynamics and mixing processes resulting from the presence of this layer are the subject of this paper. Due to the symmetry of the stream function, the fluid contains core regions surrounded by separatrix layers at both the top and the bottom of the fluid. In between the two separatrix layers lies the outer region. For simplicity, we shall study the core and separatrix layer at the bottom of the fluid; the dynamics in the upper core and separatrix layer is obtained by symmetry.

III. OVERVIEW OF TRANSPORT AND MIXING

The time-T map in Fig. 2 is obtained by plotting $\xi(\mathrm{mod}2\pi)$. The long-range transport properties of the fluid, however, are given by the wave-crest number. In Fig. 3 we plot the wave-crest number versus time obtained by numerically integrating the MW equations of motion (5) for several initial conditions along the line $\xi=0$. The solid lines are particle trajectories, and the dotted line is a point fixed in the laboratory frame. The particles in the core are trapped; hence they remain at wave crest zero and their trajectories constitute the solid horizontal line in Fig. 3.

The particles in the outer region increase their wave-crest number rapidly. Chaotic trajectories in the outer region are restricted to very thin layers by KAM curves, and hence also increase their wave-crest number rapidly and relatively constantly. By comparing with a point fixed in the laboratory frame, we see that the outer region constitutes a backflow, with particles streaming in the opposite direction of the wave propagation. These transport properties of particles in the core and outer region have been seen in experiments on traveling waves by Moses and Steinberg.[6]

The behavior of particles in the separatrix layer appears dramatically in Fig. 3; the trajectories alternate between trapped episodes, appearing as horizontal segments, and untrapped episodes, appearing as steep segments with slopes comparable to those in the outer region. Segments with shallow slopes are composed of many short trapped and untrapped episodes. Both trapped and untrapped episodes of widely varying duration are visible in the separatrix layer. The island embedded in the separatrix layer, which is visible in Fig. 2, is perpetually trapped and shall be considered to be part of the core. There also may be islands within the separatrix layer that are perpetually untrapped and are thus in the outer region. In this way, both the core and outer regions may be composed of several disconnected regions.

Particles in the core are carried large distances as they travel with the wave. Because they are trapped within the core, which is bounded by KAM curves, they do not mix with the surrounding fluid. Within the core itself, there is mixing due to isolated chaotic layers. This mixing is small since the chaotic layers are very thin for small δ. Of course, in any real system the wave train is of finite extent and the core is eventually carried to a region where the wave breaks down. At this point, it is possible that particles in the core will mix with the surrounding

fluid. In addition, due to departures from the fluid approximation, mass can slowly diffuse across KAM curves. In the context of an idealized infinite wave train, however, particles in the core experience long-range transport but do not contribute to enhanced mixing.

Particles in the outer region are trapped in the backflow and carried large distances in the opposite direction of the wave. The wave-crest velocity is constant, as seen by the fact that trajectories appear as straight lines in Fig. 3. Because the trajectories in the outer region travel at different velocities, the particles spread out as in a shear flow. The regular trajectories follow one-dimensional curves, and for small δ the chaotic layers are very thin; hence the particles do not mix with one another. As in the core, departures from the fluid approximation allow mass to cross KAM surfaces resulting in a small degree of mixing.

The separatrix layer produces both long-range transport and relatively large enhanced mixing. A single trajectory consists of a sequence of trapped and untrapped episodes of varying duration. Thus, particles are picked up and carried with the wave for a while, then they are dropped and drift backwards (with respect to both the wave and the laboratory frame) for a while, and then they are picked up again, etc. In this way, particles from widely varying regions of the fluid are mixed together. In addition, particles which start nearby spread out rapidly. As seen in Fig. 3 the mean transport of particles in the separatrix layer is in the direction of wave propagation. This process occurs even at very small values of δ. The value of δ controls the width of the separatrix layer, and hence the fraction of the fluid involved in the process, but the trapping and untrapping exist for all nonzero δ.

In the remainder of this paper we focus on the hopping between trapped and untrapped episodes. We shall use two maps to study different aspects of the dynamics: the time-T map already introduced, and the separatrix map (also called the whisker map) introduced by Chirikov[12,13] to study motion near the separatrix of the parametrically forced pendulum. The time-T map arises in the formulation of Mel'nikov's method and is the natural choice to study the role of the stable and unstable manifolds in the dynamics. The separatrix map, on the other hand, is constructed using a surface fixed in phase space and is the appropriate map when studying the statistics of the hopping. A further advantage of the separatrix map is that it is simple to construct and can be quickly iterated on a computer. We find that calculating certain aspects of the transport requires long-time statistics of the chaotic dynamics. In fact, these times are so long as to preclude direct numerical integration of the equations of motion; the speed of iteration of the separatrix map is necessary in order to obtain such long-time statistics.

IV. STABLE AND UNSTABLE MANIFOLDS

As δ is increased from zero, the fixed points on the boundary of the fluid persist in the time-T map. Although their positions on the boundary move, the time-T map must undergo a bifurcation for the fixed points to be either destroyed or change their stability properties. Due to the symmetry of the problem, the heteroclinic orbit along the boundary is not broken. The heteroclinic trajectory γ, however, is broken. Let ξ_l and ξ_r be the positions of the fixed points with $\xi<0$ and $\xi>0$, respectively. There are two manifolds of interest: W^u, the unstable manifold of the fixed point at $(\xi,\zeta)=(\xi_l,0)$, and W^s, the stable manifold of the fixed point at $(\xi,\zeta)=(\xi_r,0)$. These manifolds intersect transversely[8] for nonzero δ, indicating the existence of a Smale horseshoe. Following Channon and Lebowitz,[14] Rom-Kedar *et al.*[15] study how the lobes of such intersecting manifolds affect particle transport. They show that the time evolution of a small number of lobes determines the transport properties, allowing a significant reduction in the numerical calculation of the transport rates. Further, they show that it is the intersection of the lobes which is important for transport.

The separatrix layer in the MW can be divided into regions which are trapped and untrapped for a single iteration of the time-T map. The region which is trapped for one iteration $\mathcal{T}$ consists of those points in the separatrix layer whose wave-crest number is unchanged in time T. Similarly, those points whose wave-crest number changes in time T are untrapped and in region $\mathcal{U}$. The two regions are not invariant. The fact that the image of $\mathcal{T}$ is partially in $\mathcal{U}$, and vice versa, gives rise to the alternation between trapped and untrapped episodes. Figures 4(a)

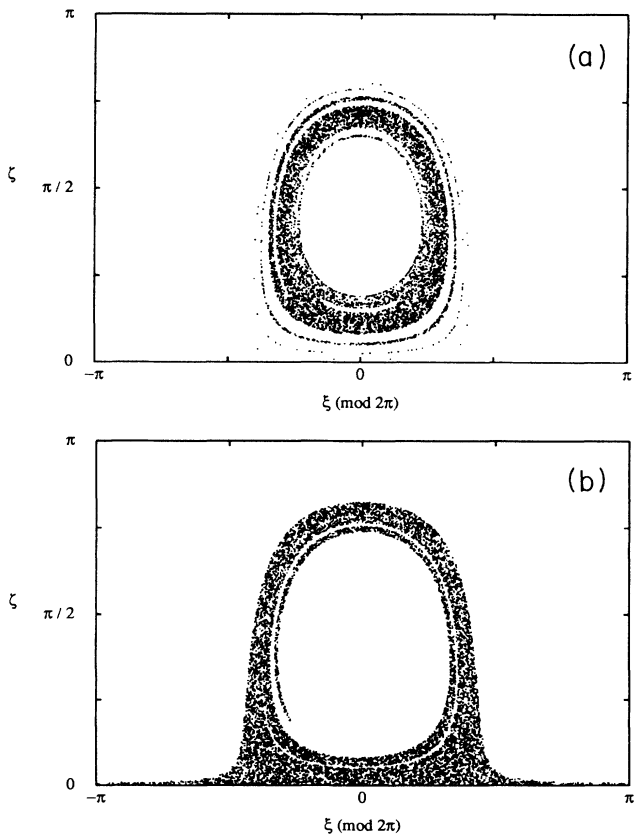

FIG. 4. (a) The region $\mathcal{T}$ which is trapped for one iteration of the MW time-T map. The parameters are those used in Fig. 2. (b) The region $\mathcal{U}$ which is untrapped for one iteration of the MW time-T map. The parameters are those used in Fig. 2.

and 4(b) show the regions $\mathcal{T}$ and $\mathcal{U}$, respectively. These regions are obtained by numerically integrating the equations of motion with $\delta=0.4$ for several initial conditions along $\xi=0$ in the separatrix layer.

The regions $\mathcal{T}$ and $\mathcal{U}$ are related to the lobes of W^s and W^u. Figure 5 is a simplified sketch of these lobes. Since L lies on the inside of W^u it contains particles that would be permanently *trapped* when $\delta=0$. However, for $\delta>0$, the lobe L is mapped into the lobe L' in one iteration of the time-T map. Since L' lies to the outside of W^s the particles in it would be permanently *untrapped* if $\delta=0$. Consequently the lobe structure determines exactly which particles become detrapped in one iteration of the time-T map. Correspondingly, there are untrappped particles which become trapped after one iteration. Thus understanding the way the various lobes map into each other under the time-T map enables one to understand the process of trapping and detrapping.[14,15]

Figures 6(a) and 6(b) show W^u for $\alpha=4.0$ and 0.195, respectively, obtained numerically by iterating 5000 initial conditions lying on the unstable manifold near ξ_l. The stable manifold W^s is obtained by reflecting W^u about $\xi=0$. When $\alpha=4.0$ [Fig. 6(a)] W^u and W^s look qualitatively like the sketch in Fig. 5, and it is easy to identify the lobes L and L'. In particular, since L' lies entirely to the left of $\xi=\pi$, the wave-crest number of the particles in L is not changed in one iteration of the time-T map. As α decreases lobe L' elongates towards larger values of ξ, eventually crossing $\xi=\pi$ and winding around the phase space cylinder. Once L' wraps around the cylinder one iteration of the time-T map will increase the wave-crest number of those particles in lobe L which lie in the preimage of the part of L' winding around the cylinder. Lobe L also responds to decreasing α by becoming more elongated, with the elongated lobe winding around the core. For any value of α, the higher-order lobes are successively more elongated, and eventually wrap around the cylinder. Thus successive iterations of the time-T map cause transport in wave-crest number even for large α. When $\alpha=0.195$ [Fig. 6(b)] even the low-order lobes are very elongated and parts of W^u appear disconnected due to the extreme stretching of the manifold and the paucity of initial conditions used. Nonetheless, we can still identify the lobes L and L'. The latter is the lobe which extends to roughly 3.5π. The lobe

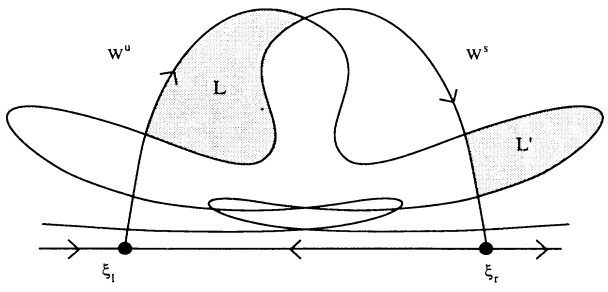

FIG. 5. Simplified sketch of the lobes created by the intersection of the manifolds W^s and W^u.

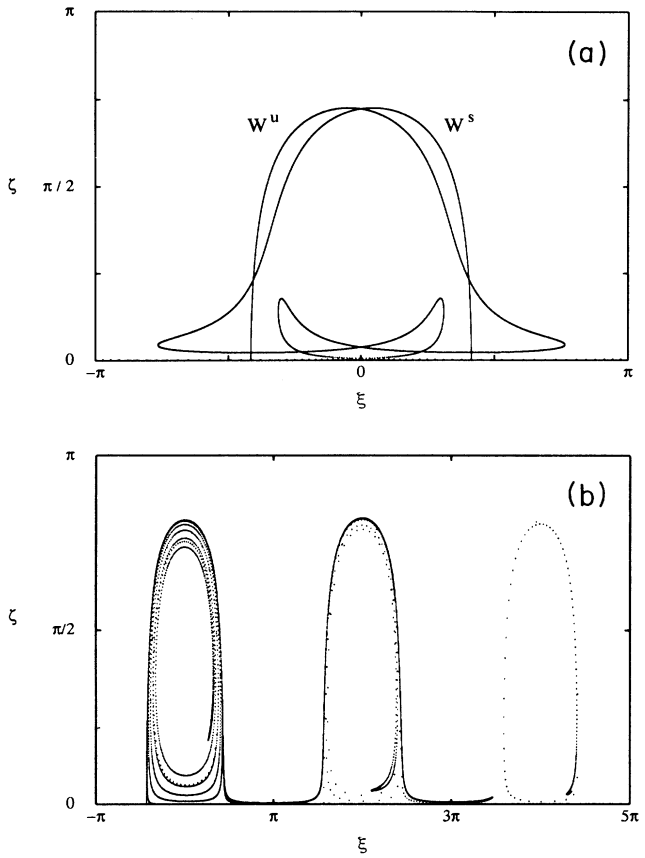

FIG. 6. (a) The manifolds W^s and W^u. W^u is obtained by iterating the MW time-T map for 5000 initial conditions near ξ_l. W^s is the reflection of W^u about $\xi=0$. The parameters are those used in Fig. 2 except $\alpha=4.0$. (b) Same as (a) except $\alpha=0.195$, and only W_u is shown.

L is its preimage under the map and is obtained by reflecting the lobe which winds several times around the core about the line $\xi=0$. Since lobe L' extends past 3π it wraps around the cylinder twice; a single iteration of the time-T map can thus increase the wave-crest number of a particle in L by zero, one, or two. Particles come to be in lobe L because they originally started in a lobe which eventually maps to L. These lobes may wind around the cylinder in the negative ξ direction, causing L to contain particles which originally had smaller wave-crest numbers. In this manner, the winding of the lobes around the phase space cylinder is responsible for transport in wave-crest number. The spatial periodicity of the MW flow means that the structure of manifolds and lobes is repeated at each wave-crest number. Successive episodes of trapped and untrapped flow are due to intersections of lobe L' and its images at one wave-crest number with lobe L and its preimages at a larger wave-crest number. For a more detailed discussion of lobe geometry and the role of lobe intersections, see Rom-Kedar *et al.*[15]

The trapped region $\mathcal{T}$ and the untrapped region $\mathcal{U}$ may be divided into disjoint regions $\mathcal{T}_n$ and $\mathcal{U}_n$ which are trapped and untrapped, respectively, for exactly n iterations of the time-T map,

$$\mathcal{T}=\bigcup_{n=1}^{\infty}\mathcal{T}_n,\quad \mathcal{T}_m\cap\mathcal{T}_n=\emptyset \text{ for } m\neq n$$
$$\mathcal{U}=\bigcup_{n=1}^{\infty}\mathcal{U}_n,\quad \mathcal{U}_m\cap\mathcal{U}_n=\emptyset \text{ for } m\neq n\ . \tag{6}$$

The action of the time-T map is to take each $\mathcal{T}_{n+1}$ into $\mathcal{T}_n$ and $\mathcal{U}_{n+1}$ into $\mathcal{U}_n$ for $n>0$. $\mathcal{T}_1$ and $\mathcal{U}_1$ are mapped into $\mathcal{U}$ and $\mathcal{T}$, respectively; the distribution of the duration of trapped and untrapped episodes is determined by the intersections of the image of $\mathcal{T}_1$ with the $\mathcal{U}_n$'s and the image of $\mathcal{U}_1$ with the $\mathcal{T}_n$'s. For example, if the image of $\mathcal{T}_1$ were entirely in $\mathcal{U}_5$ then all untrapped episodes (after the first one) would last for five iterations of the time-T map.

The time-T map, however, fails to capture some essential aspects of the dynamics. The separatrix layer encircles the core. As trajectories wind around the top of the core they approach the neighborhood of $(\xi_r,0)$ where they have two choices: they may continue with positive velocity and wind around the cylinder, or they may reverse direction and wind back around the bottom of the core. If a trajectory remains at the same wave-crest number in one iteration of the time-T map it may be because it wound around the core rather than winding around the cylinder, or it may be because the particle traveled slowly enough that it didn't make a choice in time T. On the other hand, a particle which changes its wave-crest number may have wound around the cylinder more than once in time T. A trajectory may even wind around both the core and the cylinder in time T. Thus, although the time-T map arises naturally in the study of periodically perturbed systems, it does not capture some of the crucial features of the motion near a separatrix. For this reason, we turn to the separatrix map.

V. THE SEPARATRIX MAP

The separatrix map is an approximate map obtained by considering the intersection of trajectories with a surface Σ fixed in phase space. In the two-dimensional phase space of the MW, Σ is a one-dimensional line. Although the map is insensitive to the exact surface, we choose for concreteness the surface

$$\Sigma=\{(\xi,\zeta):\zeta=|\xi-\xi_0|\}\ , \tag{7}$$

where $(\xi,\zeta)=(\pm\xi_0,0)$, $\xi_0=\cos^{-1}(1/R)$ are the positions of the fixed points of the TW. The surface is sketched in Fig. 7. In traveling from one intersection with Σ to the next a trajectory will either wind exactly once around the core and be called trapped, or wind exactly once around the cylinder and be called untrapped. The separatrix map thus captures the essential dynamics of the separatrix layer.

Two different times will be used to construct the separatrix map. The first, s^n, is the time of the nth intersection with Σ. Although necessary for the formulation of the map, s^n will not appear in the map itself. The second time t^n is the time at which the trajectory crosses $\xi=0(\mathrm{mod}2\pi)$ with positive velocity just prior to the $(n+1)$th intersection. Thus $t^n<s^{n+1}<t^{n+1}$.

For each intersection we calculate the value of the unperturbed (TW) stream function

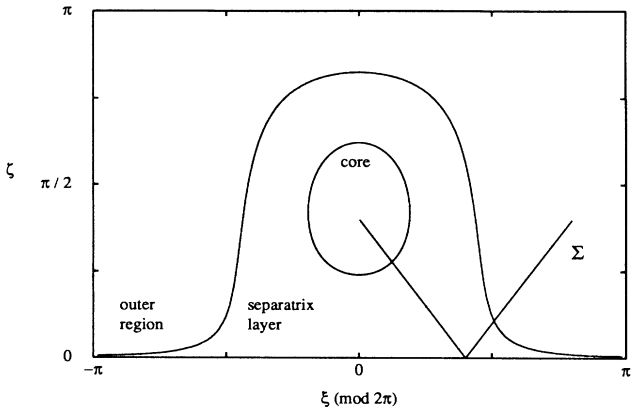

FIG. 7. Surface of section Σ used to construct the separatrix map.

$$\psi_0^n\equiv\psi_0(\xi_n,\zeta_n)\ , \tag{8}$$

where (ξ_n,ζ_n) is the position on Σ of the nth intersection. The value of the stream function at the next intersection is then

$$\psi_0^{n+1}=\psi_0^n+\int_{s^n}^{s^{n+1}}d\tau\frac{d\psi_0}{d\tau}\ . \tag{9}$$

Since the time derivative of a quantity $A(\xi,\zeta)$ at time τ is given by the Poisson bracket

$$\left.\frac{dA}{dt}\right|_{\xi,\zeta,\tau}=\{A(\xi,\zeta),\psi(\xi,\zeta,\tau)\}\ , \tag{10}$$

we can write Eq. (9) as

$$\psi_0^{n+1}=\psi_0^n+\delta\int_{s^n}^{s^{n+1}}d\tau\{\psi_0(\xi(\tau),\zeta(\tau)),\psi_1(\xi(\tau),\zeta(\tau),\tau)\}\ . \tag{11}$$

Following Chirikov[13] we approximate the change in ψ_0 by evaluating the above integral on the unperturbed separatrix, rather than along the actual trajectory. Depending on whether the particle is trapped or untrapped, it spends its time near $\zeta=0$ either traveling to the left from $\xi=\xi_r$ to $\xi=\xi_l$, or traveling to the right from $\xi=\xi_r$ to $\xi=\xi_l+2\pi$, respectively. Thus in approximating the true trajectory with the motion on the unperturbed separatrix we must integrate along different portions of the boundary $\zeta=0$ for trapped and untrapped trajectories. But since $\psi_0=\psi_1=0$ on $\zeta=0$, the contribution to Eq. (11) from the motion along $\zeta=0$ is zero and the distinction is irrelevant. The only contribution to Eq. (11) comes from integrating along the heteroclinic connection γ.

The actual trajectory takes a finite time to travel from the neighborhood of ξ_l to the neighborhood of ξ_r. On the other hand, a particle following the heteroclinic connection γ requires an infinite amount of time to travel from ξ_l to ξ_r. The replacement of integration along the

true trajectory with integration along γ is accomplished by integrating from $-\infty$ to ∞ and adjusting the phase of ψ_1 such that it has the same phase for both trajectories when $\xi=0$. The trajectory on γ is parametrized such that $\xi=0$ at $\tau=0$, while the true trajectory crosses $\xi=0$ at $\tau=t^n$. To match phases when $\xi=0$, the explicit time dependence of ψ_1 must thus be $\tau+t^n$. The resulting approximate expression is

$$\psi_0^{n+1}=\psi_0^n+\delta\int_{-\infty}^{\infty}d\tau\{\psi_0(\xi_\gamma(\tau),\zeta_\gamma(\tau)),\psi_1(\xi_\gamma(\tau),\zeta_\gamma(\tau),\tau+t^n)\}\ , \tag{12}$$

where $(\xi_\gamma(\tau),\zeta_\gamma(\tau))$ is the heteroclinic orbit γ. We now note that the integral in Eq. (12) is precisely the Mel'nikov function $M(t^n)$.[11] The new value of ψ_0 is thus approximated by

$$\psi_0^{n+1}=\psi_0^n+\delta M(t^n)\ . \tag{13}$$

The explicit form of the Mel'nikov function is[8]

$$M(t^n)=-\frac{6\alpha}{R}\sin(\alpha t^n)\int_0^{\infty}d\tau\,\zeta_\gamma(\tau)\cos(\alpha\tau)\ . \tag{14}$$

It remains to find an expression for the time t^{n+1}. In the same spirit as the approximation used above, we approximate the time for the actual trajectory to go from one crossing of $\xi=0(\mathrm{mod}2\pi)$ to the next by the time a trajectory of the unperturbed systems takes to complete one circuit of its orbit. Thus the time between t^{n+1} and t^n is approximated by the period of the unperturbed (TW) orbit with stream function ψ_0^{n+1}. The value ψ_0^{n+1} is used rather than ψ_0^n since the trajectory crosses $\xi=0$ with positive velocity just before it intersects Σ the $(n+1)$th time.

The separatrix map is thus

$$\begin{aligned}\psi_0^{n+1}&=\psi_0^n+\delta M(t^n)\ ,\\ t^{n+1}&=t^n+T(\psi_0^{n+1})\ ,\end{aligned} \tag{15}$$

where $T(\psi_0)$ is the period of the unperturbed orbit with stream function ψ_0. The approximations which go into Eq. (15), while reasonable, are rough, with no indication of the size of the corrections. The closer the true trajectories are to the unperturbed separatrix the better the approximations will be; we thus expect the map to be valid in the limit of small δ when the separatrix layer is thin. Chirikov[13] tested the validity of the separatrix map in his study of the parametrically forced pendulum by comparing it with numerical integration of the equations of motion for the case where the ratio λ of the frequency of the perturbation to the unperturbed frequency is large. He found that the agreement between the separatrix map and the numerical calculation was "satisfactory," and improved as the ratio became larger. In the MW, on the other hand, the frequency of the perturbation is α, the appropriate unperturbed frequency is $(R^2-1)^{1/2}$, the frequency of small-amplitude orbits circling the center of the core of the TW, and the ratio $\lambda=\alpha/(R^2-1)^{1/2}\ll 1$. We thus undertake our own comparison of the separatrix map with the numerically integrated MW trajectories which we shall describe below.

The map (15) so far says nothing about whether a trajectory winds around the core or the cylinder. In the TW, those trajectories with $\psi_0>0$ ($\psi_0<0$) wind around the core (cylinder). Thus we make the identification that when $\psi_0^n>0$ ($\psi_0^n<0$) the particle is trapped (untrapped) for the next iteration of the separatrix map. If the particle is trapped then the wave-crest number remains constant during the next iteration of the separatrix map, otherwise it increases by one. Note that the separatrix map differs from the time-T map discussed in Sec. IV. In the latter, the stable and unstable manifolds of a fixed point may extend over several wave crests if α is sufficiently small. Consequently, in time T a transition by more than one wave crest may occur. This process is also captured in the separatrix map since a trajectory always intersects the surface Σ whenever the wave-crest number changes. In the separatrix map, transitions by $\Delta n>1$ in wave-crest number in time T are simply those which require Δn iterations of the map before $t^{n+\Delta n}-t^n\approx T$.

The simplicity of the separatrix map is worth noting. The map depends only on the Mel'nikov function and the period of the unperturbed orbits; it can thus be used to study the dynamics whenever a homoclinic or heteroclinic orbit is broken by a perturbation. Further, because these functions can be calculated in advance and stored, numerical iteration of the separatrix map is quite rapid. In fact, iterations of the separatrix map proceed 10^4 times faster than direct numerical integration of the equations of motion.

We judge the validity of the approximations used in the separatrix map by comparing iterations of the map with direct numerical integration of the equations of motion. Figure 8(a) compares the probability distribution of trapped episode duration obtained by iterating the approximate separatrix map and integrating the exact equations of motion for $\delta=0.01$. Figure 8(b) shows a similar comparison for the distribution of untrapped episode duration. The separatrix map captures both the magnitude of the peaks and the detailed structure of the distributions, indicating that despite the roughness of the approximations it is an excellent tool for studying the dynamics of the separatrix layer. Similar results were obtained for different values of R, α, and δ. Note that this calculation verifies both the separatrix map (15) and the identification of trapped and untrapped episodes.

Figure 9 plots iterations of the separatrix map for several initial conditions. The chaotic layer around $\psi_0=0$ is the separatrix layer. The regular trajectories outside the separatrix layer are in the core when $\psi_0>0$,

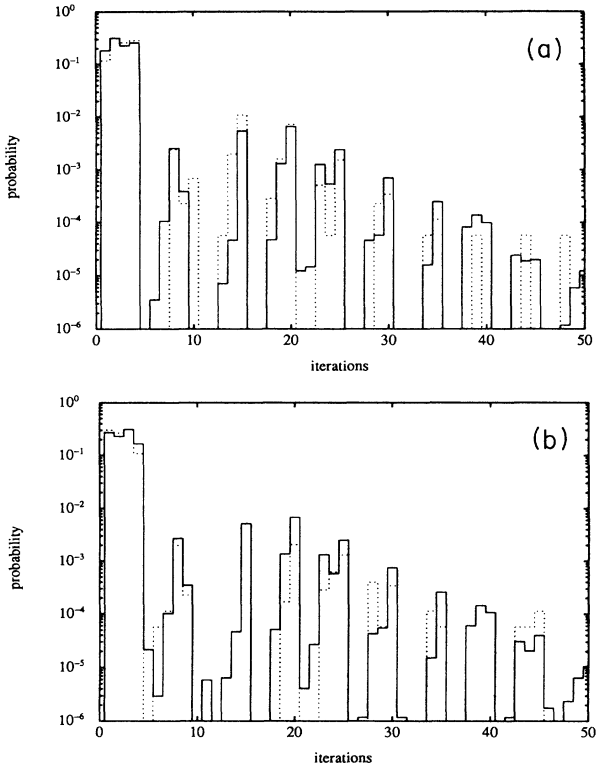

FIG. 8. (a) Comparison of the probability distribution of the duration of trapped episodes obtained by iterating the approximate separatrix map (solid line), and that obtained by numerically integrating the exact equations of motion (dotted line). The parameters used are $R=3.266$, $\alpha=0.195$, $\theta=0$, and $\delta=0.01$. (b) Same as Fig. 8(a), but for the distribution of the duration of untrapped episodes.

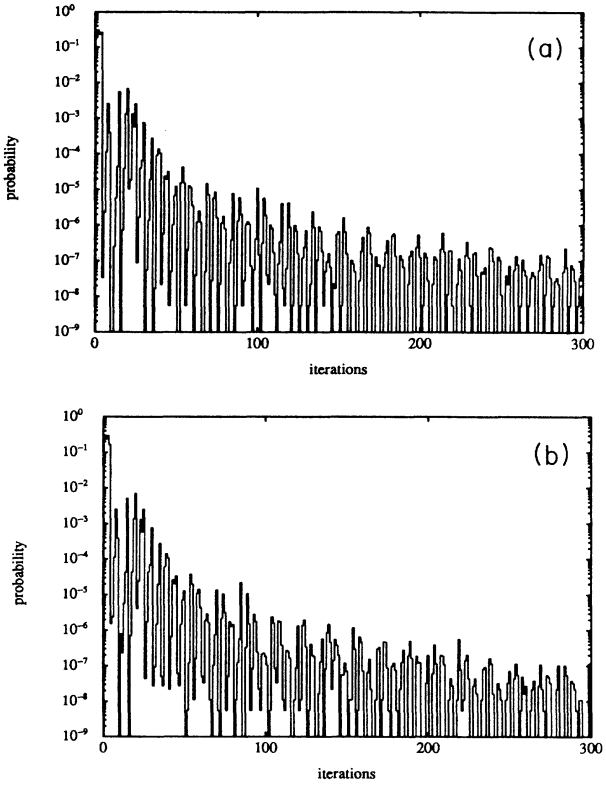

FIG. 10. (a) Probability distribution of the duration of trapped episodes calculated from the separatrix map. The parameters are those of Fig. 8(a). (b) Same as (a), but for the duration of untrapped episodes.

and in the outer region when $\psi_0<0$.

One feature of the dynamics which plays an important role in determining the transport properties is the probability distribution of the duration of trapped and untrapped episodes. These distributions are shown in Figs. 10(a) and 10(b), respectively. Note the similarity between the trapped and untrapped episode distributions. The complexity of the structure is striking; the distributions oscillate over five orders of magnitude in a few iterations. These oscillations can ultimately be traced to the irregular intersections of the lobes of the stable and unstable manifolds in the time-T map. Also of interest are the long tails in the distributions. Yet the distributions are not identical. The means of the trapped and untrapped episode distributions are 2.98 iterations and 2.77 iterations, respectively. The rms deviations are more difficult to determine precisely as they depend sensitively on rare events in the tail; approximate values are four for trapped episodes and 40 for untrapped episodes. The overall shape of the distribution's decay can be determined by smoothing the structure. Figure 11 shows the smoothed untrapped episode distribution, along with the power-law decay obtained by a least-squares fit to a log-log plot of the distribution. The decay exponents are 3.79 for the trapped episode distribution and 3.59 for the untrapped episode distribution. The smaller decay exponent and larger rms deviation indicates that long untrapped episodes are more likely than long trapped episodes. These exponents are significantly larger than those reported in related studies employing $\lambda \gg 1$.[16]

Distributions with long tails are ubiquitous in chaotic systems in which there are islands and chaotic layers.[17]

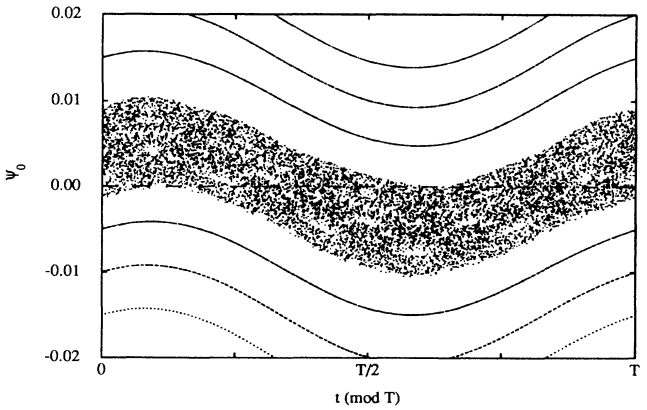

FIG. 9. Iterations of the separatrix map for several initial conditions. The parameters are those of Fig. 8(a).

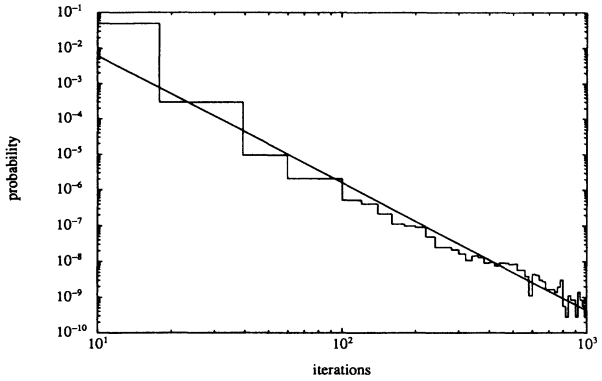

FIG. 11. Smoothed probability distribution of the duration of untrapped episodes obtained from that of Fig. 10(b) by averaging over episodes with duration of 1 to 20 iterations, 21 to 40 iterations, etc. The solid line is a fit of the smoothed distribution to a power-law decay with exponent 3.59.

Near the unbroken KAM curves which bound chaotic layers and islands are cantori which, at a slightly smaller value of the nonintegrable coupling (δ in the MW), are themselves unbroken KAM curves. These cantori appear in hierarchies, have small gaps, and are effective barriers to the motion of chaotic trajectories. Cantori generally act as barriers to motion in the direction of the action variable, while allowing motion in the angle variable. Once inside one of these cantori, a trajectory may take a long time to escape. If the trajectory manages to pass through several cantori in the hierarchy the escape time may be enormous. Thus, chaotic trajectories may shadow the KAM curves bounding a chaotic region.

By capturing trajectories near the bounding KAM curves, the cantori produce long episodes of trapped and untrapped flow. A trajectory captured behind cantori near the upper (lower) KAM curve in Fig. 9 will wind around the core (cylinder) during its stay near the boundary, and hence be trapped (untrapped). This picture is complicated by the fact that the bounding KAM curves approach $\psi=0$ (see Fig. 9). Nevertheless, the hierarchy of cantori produces a large distribution in the times for which trajectories remain near the bounding KAM curves, resulting in the long tails in the distribution of trapped and untrapped episodes.

VI. ANOMALOUS DIFFUSION

The dispersion of particles is measured by the mean square of the distance traveled

$$\Delta x^2(t)=\langle [x(t)-x(0)]^2\rangle-\langle x(t)-x(0)\rangle^2 , \tag{16}$$

where, for our purposes $x(t)$ is a one-dimensional particle trajectory and the average is over initial conditions. The dependence of $\Delta x^2(t)$ on t is often characteristic of the type of process responsible for the dispersion.

A random process such as Brownian motion induces a spreading in particle trajectories in which the mean-square distance depends linearly on the time. In this case, one can define a diffusion coefficient

$$D=\lim_{t\to\infty}\frac{\Delta x^2(t)}{t} . \tag{17}$$

On the other hand, consider an ensemble of initial conditions spread across a two-dimensional shear flow with the velocity profile

$$\begin{aligned} v_x(x,y)&=v(y) , \\ v_y(x,y)&=0 . \end{aligned} \tag{18}$$

The position at time t of a particle starting at $(x,y)=(0,y_0)$ is $(v(y_0)t,y_0)$. The horizontal spreading of particles is given by

$$\begin{aligned} \Delta x^2(t)&=\langle [v(y_0)t]^2\rangle-\langle v(y_0)t\rangle^2 , \\ &=t^2[\langle v(y_0)^2\rangle-\langle v(y_0)\rangle^2] , \end{aligned} \tag{19}$$

and depends quadratically on the time. The average in (19) is over initial conditions with different y_0. The two processes also have quite different mixing properties: in Brownian motion the particles mix rather well, while in the shear flow (18) the ordering of the particles is preserved as they spread.

In many chaotic systems it is the diffusion in action, or energy, which is physically important. For maps in which the phase space is periodic in the action as well as in the angle, accelerator modes are possible. In this case, the map may contain stable fixed points in which the action changes by $2\pi n$, where n is an integer. These fixed points and their associated islands are the accelerator modes. The cantori associated with accelerator modes can cause chaotic trajectories to shadow these islands; this results in particle streaming rather than diffusion, and leads to an infinite diffusion coefficient. In more generic mappings the phase space is not periodic in action; in this case the phase space may contain quasiaccelerator modes which exist over a finite range of action. These modes result in enhanced diffusion in action, but do not lead to singularities.

The transport in the separatrix layer of the MW differs from that discussed above in that the transport is not in a direction that changes the action. Indeed, the KAM curves which bound the separatrix layer restrict the trajectories to a rather narrow band in action. Neither is the physically relevant transport in the angle direction; particles in the core, for example, have a monotonically increasing angle, but remain trapped by the wave forever. It is the spreading of trajectories in wave-crest number which causes mixing over large regions of the fluid. The cantori near the bounding KAM surfaces do, however, play a role similar to those near accelerator modes: trajectories can penetrate the cantori and remain there for a long time before exiting, resulting in trapped and untrapped episodes of large duration. Because of the possibility of an infinite diffusion coefficient, we focus on the diffusion exponent ν,

$$\Delta x^2(t)\sim t^{\nu} \text{ as } t\to\infty . \tag{20}$$

More precisely, we study $\Delta x^2(N)$ as N, the number of iterations of the separatrix map, becomes large. This gives the same exponent as measuring $\Delta x^2(t)$ since, as

verified numerically, for large N the fluctuations in the time between individual iterations of the map average to zero and t equals N times the average time between iterations. An exponent greater than one indicates an infinite diffusion coefficient and characterizes *anomalous diffusion.*

We have numerically measured the diffusion exponent for particles in the separatrix layer. The spread of particles is strongly influenced by episodes of long duration; one must therefore use very long trajectories to accurately measure the exponent. The average is performed on 1000 initial conditions within the separatrix layer with initial time $t^0=0$ and random initial ψ_0. The mean square deviation of the wave crest number over N iterations of the separatrix map is then fit to a power law. The resulting exponent ν is plotted versus N in Fig. 12; we judge that the exponent is close to its asymptotic value when $N=3.2\times10^6$. This large value of N precludes the possibility of measuring the diffusion exponent by direct numerical integration of the equations of motion. One must take into account the fact that an initial condition may lie within an island embedded in the separatrix layer, and thus be perpetually trapped or untrapped, and properly in the core or outer region, respectively. In Fig. 12 the $\times$'s are averages over all initial conditions, while the $\circ$'s average over only those initial conditions that make at least one trapped or untrapped transition, indicating they are not within such an island. Since N is necessarily finite, this procedure counts some initial conditions as being in islands although they are actually in the separatrix layer. The true diffusion exponent for the separatrix layer is thus between the $\times$'s and $\circ$'s, but approaches the $\circ$'s as $N\to\infty$. The error due to using a finite number of initial conditions is indicated by plotting the exponent calculated from two different ensembles for each N. We estimate a value of 1.93 for the diffusion exponent, indicating the existence of anomalous diffusion. Thus, in terms of the time dependence of the transport, the separatrix layer is closer to a shear flow than to a standard diffusive process. Unlike a shear flow, however, particles in the separatrix layer become well mixed by the trapping and untrapping process.

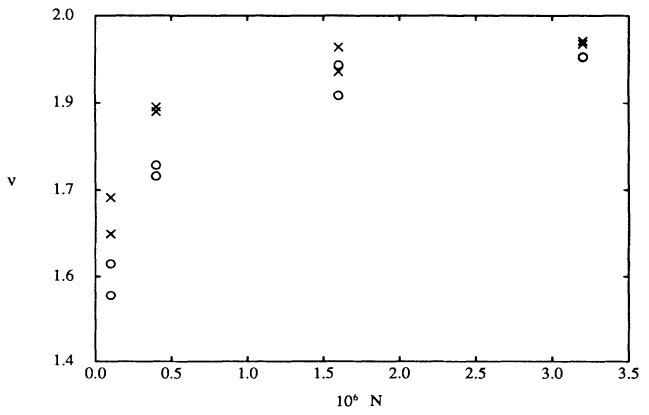

FIG. 12. Diffusion exponent ν vs number of iterations of the map N. The $\times$'s result from averages over all initial conditions, while the $\circ$'s result from averages over only those initial conditions which make at least one trapped or untrapped transition. The results are shown for two different realizations of 1000 random initial conditions. The parameters are those of Fig. 8(a).

VII. DISCUSSION

The TW and MW stream functions studied above, Eqs. (2) and (3), respectively, do not satisfy the correct experimental boundary conditions for binary fluid convection. The phenomena described in this paper are, however, due to structures which are typical of nonintegrable Hamiltonian systems, and thus should persist in flows with realistic boundaries. For example, Moses and Steinberg[6] propose a TW stream function which satisfies rigid boundary conditions, but unlike the stream function (2) does not satisfy the dynamical equations. This stream function has a fixed point inside the fluid with a homoclinic orbit, and thus, like the TW (2), has core and outer regions. In their experiment, Moses and Steinberg[6] observe transport which is similar to that of the TW (2). In the event of either a second Hopf bifurcation or an external time-dependent perturbation, we expect the homoclinic connection to break; if the resulting manifolds intersect transversely then the homoclinic orbit will be replaced by a chaotic separatrix layer. There will be trapped and untrapped episodes, and the transport and mixing will be similar to that described above.

In this paper we have used techniques from dynamical systems theory to study the transport and mixing in such quasiperiodic waves. The Eulerian flow is simple and resides on a 2-torus, while the Lagrangian flow is highly structured, containing KAM curves, cantori, island chains, and chaos. We find that there is a chaotic separatrix layer in which particles alternate between being trapped and carried with the wave and being untrapped and flowing backwards with respect to both the wave and laboratory frame. By trapping and untrapping particles for varying lengths of time the separatrix layer mixes fluid particles across large distances. Further, the trapping and untrapping produces long-range transport in physical space, and, due to the presence of cantori, anomalous diffusion. The transport and diffusion studied here differ from that in most previously studied chaotic systems in that it is transport and diffusion in wave-crest number, and hence physical space, rather than in action. Since the structures producing these phenomena are typical of nonintegrable Hamiltonian systems, we expect long-range transport, anomalous diffusion, and enhanced mixing to be common properties of two-dimensional quasiperiodic waves with broken homoclinic or heteroclinic orbits.

ACKNOWLEDGMENTS

This work was supported in part by the California Space Agency and the National Science Foundation under Grant No. DMS-8814702. We are grateful to A. Lichtenberg and J. D. Meiss for several helpful comments and suggestions.

*Present address: National Center for Atmospheric Research–Advanced Study Program, P.O. Box 3000, Boulder, CO 80307.

[1]J. Lighthill, *Waves in Fluids* (Cambridge University Press, Cambridge, 1978).

[2]E. Knobloch and J. B. Weiss, in *The Internal Solar Angular Velocity,* edited by B. R. Durney and S. Sofia (D. Reidel, Worwell, MA, 1987), pp. 221–228.

[3]H. Aref, J. Fluid Mech. **143**, 1 (1984).

[4]R. W. Walden, P. Kolodner, A. Passner, and C. M. Surko, Phys. Rev. Lett. **55**, 496 (1985); P. Kolodner, A. Passner, C. M. Surko, and R. W. Walden, *ibid.* **56**, 2621 (1986); E. Moses and V. Steinberg, Phys. Rev. A **34**, 693 (1986); E. Moses, J. Feinberg, and V. Steinberg, *ibid.* **35**, 2757 (1987).

[5]R. Heinrichs, G. Ahlers, and D. S. Cannell, Phys. Rev. A **35**, 2761 (1987).

[6]E. Moses and V. Steinberg, Phys. Rev. Lett. **60**, 2030 (1988).

[7]E. Knobloch, Phys. Rev. A **34**, 1538 (1986).

[8]E. Knobloch and J. B. Weiss, Phys. Rev. A **36**, 1522 (1987).

[9]J. P. Gollub and T. H. Solomon, in *Chaos and Related Nonlinear Phenomena: Where Do We Go From Here?,* Proceedings of the Fritz Haber International Symposium, edited by I. Procaccia (Plenum, New York, 1987); T. H. Solomon and J. P. Gollub, Phys. Rev. A **38**, 6280 (1988).

[10]T. Geisel, A. Zacherl, and G. Radons, Phys. Rev. Lett. **59**, 2503 (1987); T. Geisel, A. Zacherl, and G. Radons, Z. Phys. B **71**, 117 (1988).

[11]J. Guckenheimer and P. Holmes, *Nonlinear Oscillations, Dynamical Systems, and Bifurcations of Vector Fields* (Springer-Verlag, Berlin, 1983).

[12]A. J. Lichtenberg and M. A. Lieberman, *Regular and Stochastic Motion* (Springer-Verlag, New York, 1983).

[13]B. V. Chirikov, Phys. Rep. **52**, 263 (1979).

[14]S. R. Channon and J. L. Lebowitz, Ann. N.Y. Acad. Sci. **357**, 108 (1980).

[15]V. Rom-Kedar, A. Leonard, and S. Wiggins (unpublished); V. Rom-Kedar and S. Wiggins (unpublished). The systems studied by Rom-Kedar *et al.* differ from the MW flow studied here in that they are not spatially periodic.

[16]B. V. Chirikov and D. L. Shepelyanski, Princeton Plasma Physics Laboratory Report No. PPP-TRANS-133 (1983); B. V. Chirikov and D. L. Shepelyanski, Physica D **13**, 395 (1984); C. F. F. Karney, *ibid.* **8**, 360 (1983).

[17]J. D. Meiss, J. R. Cary, C. Grebogi, J. D. Crawford, A. N. Kaufman, and H. D. I. Abarbanel, Physica D **6**, 375 (1983); F. Vivaldi, G. Casati, and I. Guarneri, Phys. Rev. Lett. **51**, 727 (1983); J. D. Meiss and E. Ott, *ibid.* **55**, 2741 (1985); K.-C. Lee, *ibid.* **60**, 1991 (1988).